



**University of  
Zurich** UZH

**Zurich Open Repository and  
Archive**

University of Zurich  
University Library  
Strickhofstrasse 39  
CH-8057 Zurich  
[www.zora.uzh.ch](http://www.zora.uzh.ch)

---

Year: 2014

---

## **Prolidase is required for early trafficking events during influenza a virus entry**

Pohl, M O ; Edinger, T O ; Stertz, S

DOI: <https://doi.org/10.1128/JVI.00800-14>

Posted at the Zurich Open Repository and Archive, University of Zurich

ZORA URL: <https://doi.org/10.5167/uzh-101527>

Journal Article

Accepted Version

Originally published at:

Pohl, M O; Edinger, T O; Stertz, S (2014). Prolidase is required for early trafficking events during influenza a virus entry. *Journal of Virology*, 88(19):11271-11283.

DOI: <https://doi.org/10.1128/JVI.00800-14>

1 **Prolidase (PEPD) is required for early trafficking events during influenza A**  
2 **virus entry**

3

4 **Running title: Role of PEPD as influenza A virus entry factor**

5

6

7 Marie O. Pohl<sup>1;2</sup>, Thomas O. Edinger<sup>1;2</sup> and Silke Stertz<sup>1\*</sup>

8

9 <sup>1</sup> Institute of Medical Virology, University of Zurich, 8057 Zurich, Switzerland,

10 <sup>2</sup> Life Sciences Zurich Graduate School, ETH and University of Zürich, 8057

11 Zurich, Switzerland

12

13 \* corresponding author: Silke Stertz, Ph.D.

14 e-mail: stertz.silke@virology.uzh.ch

15 phone: +41 44 634 2899

16 fax: +41 44 634 4967

17 **Abstract**

18 Influenza A virus (IAV) entry is a multi-step process that requires the interaction  
19 of the virus with numerous host factors. In this study, we demonstrate that  
20 prolidase (PEPD) is a cellular factor required by IAV for successful entry into  
21 target cells. PEPD was selected as a candidate during an entry screen  
22 performed on non-validated primary hits from previously published genome-wide  
23 siRNA screens. siRNA-mediated depletion of PEPD resulted in decreased  
24 growth of IAV during mono- and multi-cycle growth. This growth defect was  
25 independent of cell type or virus strain. Furthermore, IAV restriction was apparent  
26 as early as 3h post-infection and experiments in the absence of protein  
27 biosynthesis revealed that nuclear import of viral ribonucleoprotein complexes  
28 (vRNPs) was already blocked in the absence of PEPD. These results led us to  
29 investigate which step during entry was affected. Receptor expression, IAV  
30 attachment or internalization were not dependent on the presence of PEPD.  
31 However, when looking at the distribution of incoming IAV particles in PEPD  
32 knockdown cells, we found a localization pattern that differed compared to  
33 control cells: IAV mostly localized to the cell periphery and consequently, viral  
34 particles displayed reduced co-localization with early and late endosome markers  
35 and fusion between viral and endosomal membranes was strongly reduced.  
36 Finally, experiments using a competitive inhibitor of PEPD catalytic activity  
37 suggest that the enzymatic function of the dipeptidase is required for its proviral  
38 effect on IAV entry. In sum, this study establishes PEPD as a novel entry factor  
39 required for early endosomal trafficking of IAV.

40 **Importance**

41 Influenza A virus (IAV) continues to be a constant threat to public health. As IAV  
42 relies on its host cell for replication the identification of host factors required by  
43 the virus is of importance: First, such studies often reveal novel functions of  
44 cellular factors and can extend our knowledge of cellular processes. Second, we  
45 can further our understanding of processes that are required for entry of IAV into  
46 target cells. Third, the identification of host factors that contribute to IAV entry will  
47 enlarge the number of potential targets for the development of novel antiviral  
48 drugs that are of urgent need. Our study identifies prolidase (PEPD) as a novel  
49 entry factor of IAV required for correct routing within the endosomal compartment  
50 following virus internalization. Thereby, we link PEPD which has been shown to  
51 play a role during collagen recycling and growth factor signaling, to early events  
52 of viral infection.

53

## 54 **Introduction**

55 Influenza A virus (IAV), causes an acute febrile illness in humans generally  
56 referred to as the flu. The virus is responsible for causing annual epidemics and  
57 occasional pandemics which pose a threat to public health and a large economic  
58 burden on society. IAV belongs to the family of *Orthomyxoviridae* and contains a  
59 segmented, single-stranded RNA genome of negative polarity (1). IAV virions are  
60 enveloped and four membrane-associated proteins have been described:  
61 Hemagglutinin (HA), Neuraminidase (NA), the Matrix protein 2 (M2) ion channel  
62 (1) and the M2-related protein M42 (2). While NA is required for budding and  
63 release of viral progeny from infected cells, HA and M2 mediate entry of IAV  
64 virions into target cells which are thought to be primarily epithelial cells of the  
65 respiratory tract expressing sialic acid (3). Entry of IAV is a dynamic multi-step  
66 process that can be divided into several distinctive stages: attachment to the cell  
67 surface, internalization, endosomal transport of virions towards the perinuclear  
68 region, fusion, uncoating and import of the viral ribonucleoprotein complexes  
69 (vRNPs) into the nucleus (4). The receptor for IAV attachment is sialic acid (1).  
70 HA binds to sialic acid residues present on many cell-surface glycoproteins which  
71 triggers uptake of virions into target cells. Internalization occurs mainly via  
72 clathrin-mediated endocytosis (5-7) but also alternative pathways such as  
73 macropinocytosis have been proposed (8, 9). The pH-drop that occurs during the  
74 maturation process from early endosomes (EE) to late endosomes (LE) is  
75 required for a conformational change of HA which mediates fusion of viral and  
76 endosomal membranes (10-12). Simultaneously, the M2 ion channel allows flux

77 of protons from the endosomal compartment into the virion core (13). The  
78 resulting acidification of the virion is required for release of the vRNPs into the  
79 cytoplasm, a process referred to as uncoating (14). Finally, vRNPs are imported  
80 into the nucleus, the site of viral replication, via the karyopherin transport  
81 pathway (1, 15).

82 Vaccines against IAV are available and are the best option at present to prevent  
83 seasonal epidemics. However, these vaccines induce only short-lived protection  
84 against a small set of viruses. They do not provide protection against new strains  
85 of IAV that occasionally arise in the human population. For such a scenario it is  
86 crucial to have anti-influenza virus drugs available. Currently, there are two  
87 different classes of antiviral drugs approved for the use in humans. One class are  
88 the adamantanes which target the M2 ion channel thereby preventing uncoating  
89 (16-18). The second class of drugs targets NA and inhibits egress of the virus  
90 from the host cell (19, 20). Unfortunately, resistance of IAV against these drugs  
91 has become a major problem such that the adamantanes are not recommended  
92 for the use in humans anymore (21). In addition, virus strains resistant against  
93 NA inhibitors have been reported (22). These developments emphasize the  
94 urgent need for novel antiviral treatment options. To circumvent the problem of  
95 resistance and to increase the number of potential targets of novel antivirals,  
96 several studies are currently directed towards finding cellular proteins instead of  
97 viral proteins as drug targets. Genome-wide siRNA screens are a powerful tool to  
98 identify host factors associated with viral infections. Several such screens have  
99 been performed to determine cellular factors required by IAV during infection (23-

100 30). Surprisingly, there was hardly any overlap between the primary hits  
101 identified in these screens (31). Responsible for these discrepancies are likely  
102 the different experimental designs as well as the selection criteria and validation  
103 methodologies applied in the screens. This complicates the comparison between  
104 hits from different screens and may account for the small overlap observed. For  
105 follow-up studies, the factors that show up in several screens are thus far the  
106 best candidates. In this study, we aimed to revisit the overlapping primary hits  
107 from the different screens that had not been validated yet and screen them for a  
108 role during IAV entry. We identified PEPD, a cytosolic dipeptidase, as a novel  
109 entry factor of IAV and show that the distribution of incoming viruses was altered  
110 in cells lacking PEPD and that there were fewer viruses present in the  
111 endosomal compartment. These data indicate that the routing of IAV following  
112 internalization is likely to be dependent on PEPD. Finally, we show that the  
113 catalytic activity of PEPD may be required for the observed pro-viral effect of  
114 PEPD on IAV entry.

115

116 **Materials and Methods**

117 **Cells, viruses, and compounds.** A549, MDCK and WI38 cell lines were  
118 maintained in 10% FCS-supplemented DMEM containing penicillin/streptomycin  
119 (Life Technologies). Influenza virus strain A/WSN/33 was grown in A549 cells,  
120 while A/Hong Kong/68, FPV/Dobson and A/Panama/2007/99 were grown in  
121 embryonated chicken eggs. A/Netherlands/602/2009 was grown in MDCK cells.  
122 Purified A/PR/8/34 was purchased from Charles River. All influenza virus stocks  
123 were titered by plaque assay using Vero or MDCK cells. Virus-like particles (VLP)  
124 were generated by transfecting 293T cells with a plasmid containing an HIV  
125 provirus encoding *Gaussia* luciferase, an HIV gag-pol expression plasmid and  
126 plasmids coding for the respective viral glycoproteins (WSN-HA/NA, LASV-GP or  
127 MLV-Env) using jetPRIME (Polyplus transfection) (28). The following compounds  
128 were used: Bafilomycin A1 (Sigma-Aldrich), N-Benzylloxycarbonyl-L-proline  
129 (Chemos GmbH), cycloheximide (Sigma-Aldrich), recombinant PEPD (Abnova)  
130 and IFN-alfa 2a from Roche (Roferon-A).

131 **siRNA transfections and cell viability assay.** Cells were transfected in  
132 suspension with 30 nM siRNA (Qiagen) diluted in Opti-MEM (Life Technologies)  
133 using RNAimax (Invitrogen). 48h post-transfection cells were either infected or  
134 cell viability was determined using CellTiter-Glo (Promega). For siRNA and DNA  
135 co-transfection, A549 cells were transfected with 30nM siRNA and 200ng of  
136 plasmid DNA diluted in Opti-MEM using Lipofectamine 2000 reagent (Life  
137 Technologies).

138



139 **Entry screen and virus-like particle infection.** Per factor, four siRNAs (Qiagen,  
140 see suppl. Table 1) were used for transfection into A549 cells. Only two siRNAs  
141 per gene were used if siRNAs were functionally verified by Qiagen. 48h post-  
142 transfection, cells were infected with VLPs diluted in Opti-MEM for 1h at 37°C.  
143 Cells were washed with phosphate-buffered saline (PBS) and then kept in DMEM  
144 supplemented with 10% FCS and penicillin/streptomycin for 30h at 37°C.  
145 Luciferase activity in the supernatants was determined using the Renilla  
146 Luciferase Assay System (Promega). siRNAs that induced reductions in cell  
147 viability of more than 30% compared to siScr treatment were excluded from the  
148 analysis. The quality of reduction in IAV VLP entry was scored based on the  
149 fulfillment of the following criteria: A reduction in IAV VLP entry of more than 50%  
150 compared to control, while LASV or MLV VLP entry was higher than 50% scored  
151 1. To score 2, luciferase counts had to be below 30% compared to control for IAV  
152 VLPs while the reduction for either LASV or MLV VLPs was less than 70%.  
153 Finally, the highest score of 3 was given if siRNA-transfection resulted in  
154 reductions of IAV VLP entry of more than 70% of the control values while LASV  
155 or MLV VLP entry was not reduced more than 50% compared to siScr-treated  
156 cells. A gene was considered an entry factor if at least 2 siRNAs fulfilled one of  
157 the three criteria. With these criteria we aimed to find IAV-specific host factors.  
158 We included scoring of control VLPs (LASV and MLV) because effects on the  
159 luciferase activity following infection with these VLPs would indicate either  
160 general effects on viral entry mechanisms or effects on the retroviral steps during  
161 this assay. Next, the sum of all scores obtained for a given factor was calculated.

162 This was then multiplied with the ratio (R) of the number of successful siRNAs to  
163 the total number of siRNAs tested for a given factor.

164 **Influenza A virus infection.** A549 or WI38 cells were washed once with PBS,  
165 then infected with the respective amount of virus diluted in PBS supplemented  
166 with 0.02 mM Mg<sup>2+</sup>, 0.01 mM Ca<sup>2+</sup>, 0.3% bovine serum albumin (BSA) and 1%  
167 penicillin/streptomycin (infection PBS) at 37°C for 1h before changing to DMEM  
168 containing 0.3% BSA, 20 mM HEPES and 1% penicillin/streptomycin (post-  
169 infection DMEM). With the exception of A/WSN/33 all virus strains were grown in  
170 the presence of 0.25 ug/ml TPCK trypsin (Sigma-Aldrich). Virus titers in tissue  
171 culture supernatants were determined by standard plaque assay on Vero or  
172 MDCK cells.

173

174 **Western blotting.** Cell extracts were prepared using Laemmli buffer (62.5 mM  
175 Tris-HCl pH 6.8, 25% glycerol, 2% SDS, 350mM DTT, 0.01% Bromophenol  
176 Blue). Samples were subjected to standard SDS-PAGE and proteins were  
177 transferred to nitrocellulose membranes (Hybond ECL, GE Healthcare). For  
178 blocking, 5% milk diluted in Tris-buffered saline containing 0.5% Tween 20 was  
179 used. The following primary antibodies were used: rabbit monoclonal anti-PEPD  
180 (Abcam, ab86507); mouse monoclonal anti-MxA (kind gift of J. Pavlovic); mouse  
181 monoclonal anti-β-actin (Santa Cruz Biotechnology, sc-47778); rabbit polyclonal  
182 anti-NP (kind gift of A. Nieto); mouse monoclonal anti-M1 (kind gift of J.  
183 Pavlovic).

184 **Immunofluorescence.** To synchronize infection, A549 cells were infected with  
185 A/WSN/33 on ice for 1h. Then, cells were shifted to 37°C for the indicated times  
186 to allow infection to proceed. For NP staining, cells were fixed with 3.7%  
187 paraformaldehyde (PFA) in PBS, permeabilized with 0.5% Triton-X-100 and  
188 blocked with 2% bovine albumine. Cells were incubated with mouse monoclonal  
189 anti-NP (kind gift of J. Pavlovic). The NP/EEA1 or LBPA co-staining was  
190 performed in PBS supplemented with 50 mM NH<sub>4</sub>Cl, 0.1% saponin and 2%  
191 bovine albumine (confocal buffer). The following primary antibodies diluted in  
192 confocal buffer were used: rabbit monoclonal anti-NP (kind gift of P. Palese);  
193 mouse monoclonal anti-EEA1 (BD Biosciences) and mouse monoclonal anti-  
194 LBPA (Echelon), followed by secondary antibodies (Life Technologies, A-21121,  
195 A-21134 and A-11008). Nuclei were visualized using DAPI (Life Technologies) or  
196 DAPI Fluoromount G (Southern Biotech #0100-20). For labeling acidic organelles  
197 a LysoTracker system was used (Life Technologies LysoTracker Red DND-99,  
198 L7528). Images were acquired with a Leica SP5 confocal laser-scanning  
199 microscope. Image processing was performed using LAS AF lite Software  
200 (Leica), Imaris (co-localization and z-stack analysis) and ImageJ (nuclear signal  
201 intensity analysis and fusion site analysis). A Mann-Whitney test was used to test  
202 for significant differences in mean nuclear fluorescence intensity.

203 **Internalization assay and FACS.** A/WSN/33 was concentrated over a sucrose  
204 cushion (30%) and biotinylated using the EZ-link NHS-SS Biotin kit (Thermo  
205 Scientific). siRNA-transfected A549 cells were detached (EDTA-Trypsin, Life  
206 Technologies) and cooled down in FACS buffer (PBS supplemented with 2%

207 BSA) on ice. Cells were infected on ice with biotinylated A/WSN/33 for 1h and  
208 washed thoroughly with FACS buffer. Before cells were incubated at 37°C for 30  
209 minutes, cells were incubated on ice either with FACS buffer containing  
210 unconjugated streptavidin (2 mg/ml, Life Technologies) or FACS buffer alone.  
211 Following internalization, cells were either directly fixed with PFA (3%) or  
212 incubated with FACS buffer supplemented with streptavidin and sodium azide  
213 0.1% for 30 minutes and then fixed. For permeabilization Triton X-100 0.5%  
214 diluted in PBS was used. For staining, Cy3-labeled streptavidin (Life  
215 Technologies) diluted in FACS buffer was used. Sialic acid was stained using  
216 *Sambucus nigra* and *Maackia amurensis* lectins (Reactolab SA). FACS analysis  
217 was performed on a CyAn ADP Analyzer (Beckmann Coulter Inc.) and data were  
218 analyzed using FlowJo software.

219

220 **Fusion Assay.** Measurement of viral fusion was performed according to the  
221 protocol previously described in (32). In brief, IAV A/PR/8/34 was labeled using  
222 two fluorescent dyes, R18 and SP-DiOC18 (Molecular Probes), in a ratio 1:2 with  
223 final concentrations of R18=22  $\mu$ M and SP-DiOC18=46  $\mu$ M. After intense  
224 vortexing for 1 hour labeled virus was filtered through a 0.22  $\mu$ m pore filter. Virus  
225 was cold-bound to the cells for 30 min and after washing with PBS temperature  
226 was shifted to 37 °C for either 0, 90 or 180 minutes. Unfixed and  
227 unpermeabilized samples were mounted with DAPI Fluoromount G and images  
228 were acquired on a Leica SP5 confocal laser scanning microscope. Image  
229 analysis was carried out using the spot analysis function of Image J for SP-

230 DiOC18 staining with a distinct spot size of 20 pixels and a subsequent  
231 correction for cell numbers.

## 232 **Results**

### 233 **PEPD was identified as a potential entry factor during a virus-like particle** 234 **based entry screen.**

235 The above described genome-wide siRNA screens identified numerous factors to  
236 be involved in IAV infection. To uncover potential entry factors of IAV, we  
237 decided to revisit the primary hits of four published siRNA screens (24-26, 28)  
238 that lacked experimental validation and screen them for a role during the IAV  
239 entry process. We included only those factors that were identified during at least  
240 two (or more) out of the four published screens in order to increase the  
241 confidence of finding an association with IAV infection. As we were primarily  
242 interested in virus entry we excluded factors with a known nuclear function such  
243 as splicing factors (Fig 1A). The remaining 43 factors were screened for a role  
244 during IAV entry using a virus-like particle (VLP)-based entry assay: We used  
245 VLPs that carry IAV glycoproteins on their surface and contain a reporter gene  
246 for convenient readout. These VLPs mimic IAV particles but carry a *Gaussia*  
247 luciferase reporter gene. Human lung A549 cells were transfected with siRNAs to  
248 achieve knockdown of the respective candidate genes. Per factor, four different  
249 siRNAs were used to exclude off-target effects. 48 hours post-transfection, cells  
250 were infected with VLPs and luciferase counts were measured 30 hours post-  
251 infection as an indicator of entry efficiency. To counterscreen for non-entry  
252 related effects, VLPs carrying the envelopes of Lassa virus (LASV) or Murine

253 Leukemia virus (MLV) were included. LASV also enters target cells by  
254 endocytosis but bypasses early steps of endosomal trafficking (33). In contrast,  
255 MLV is known to enter target cells via membrane fusion (34). Entry factors were  
256 defined as genes that, upon knockdown with at least two siRNAs, resulted in  
257 inhibition of IAV-VLP entry but not of VLPs carrying glycoproteins of LASV or  
258 MLV. In total, 22 factors were shown to be associated with IAV entry (Fig 1A and  
259 B). We calculated an entry score that is based on the number of siRNAs per  
260 gene that induced IAV-specific reduction of VLP entry and the degree of  
261 reduction compared to controls. The entry score was subsequently used to rank  
262 the identified entry factors (Fig 1B). siRNAs targeting subunits of the endosomal  
263 vATPase reduced IAV VLP entry most strongly (Fig 1B and C). The vATPase  
264 mediates the acidification of endosomes and is known to be required for efficient  
265 entry of IAV (35, 36) thereby acting as internal control for our entry screen.  
266 Another well-performing candidate was prolidase (PEPD), a ubiquitously  
267 expressed cytosolic peptidase that cleaves dipeptides with a proline or  
268 hydroxyproline at the C-terminus. Three out of four PEPD-specific siRNAs  
269 potently reduced IAV VLP entry but not control VLPs (Fig 1C and Suppl. Table  
270 1). Besides its dipeptidase function, PEPD has been shown to be involved in  
271 epidermal growth factor receptor (EGFR) family signalling (37, 38). EGFR  
272 signalling is believed to play a role during IAV infections (39, 40). In addition,  
273 gene ontology analysis of the validated hits of the siRNA screens revealed  
274 kinase signalling as the most overrepresented category (31). Therefore, we  
275 chose PEPD as a candidate for follow-up studies. Efficient knockdown of

276 endogenous as well as overexpressed PEPD protein levels were confirmed by  
277 western blot (Fig 1D). Moreover, cell viability 48h after siRNA transfection was  
278 assessed to exclude false-positive effects due to increased cell death (Fig 1E).  
279 To exclude that siRNA transfection alone stimulated interferon (IFN) production,  
280 thereby reducing VLP entry in PEPD knockdown cells due to expression of  
281 antiviral genes, we detected protein levels of MxA, an IFN-inducible gene, in  
282 A549 cells 48h after siRNA transfection. No MxA induction was observed in  
283 siPEPD or siScr transfected cells. Only following stimulation with IFN, MxA was  
284 detectable (Fig 1F). These data suggest that PEPD is required during the IAV  
285 entry process and we therefore selected PEPD as a candidate for follow-up  
286 studies on IAV entry.

#### 287 **PEPD is required for growth of IAV.**

288 Next, we investigated whether knockdown of PEPD also affected growth of wild-  
289 type IAV. We transfected A549 cells with siRNAs targeting PEPD or with a  
290 control siRNA. Cells were infected with A/WSN/33 with a low MOI (0.01) to allow  
291 multi-cycle growth. 24 hours post-infection, tissue culture supernatants were  
292 harvested and viral titers were determined by plaque assay. Depletion of PEPD  
293 reduced viral titers strongly compared to siScr transfected cells (Fig 2A). Similar  
294 growth defects of A/WSN/33 were observed in WI38 cells, a primary lung  
295 fibroblast cell line (Fig 2B). In addition, IAV strains FPV/Dobson (H7N7), A/Hong  
296 Kong/68 (H3N2), A/Netherlands/602/2009 (H1N1) and A/Panama/2007/99  
297 (H3N2) also displayed reduced growth in A549 cells upon PEPD knockdown (Fig

298 2C-F), indicating that the observed phenotype is virus strain and cell line  
299 independent.

### 300 **Depletion of PEPD affects an early step during the IAV life cycle.**

301 To determine whether IAV growth is also affected during mono-cycle growth, we  
302 monitored viral protein production 6h post infection in siRNA-treated A549 cells.  
303 Knockdown of PEPD resulted in decreased protein levels of M1 in western blot  
304 analysis (Fig 3A). Next, siRNA transfected A549 cells were infected with  
305 A/WSN/33 with a high MOI (10) for 3h and viral NP protein expression was  
306 visualized by confocal microscopy. In siScr treated cells, a strong NP signal was  
307 detected in the nuclei of infected cells (Fig 3B) while in cells depleted of vATPase  
308 barely any nuclear NP was detectable. Following transfection of siRNAs targeting  
309 PEPD, nuclear NP expression was largely absent, similar to vATPase  
310 knockdown cells. The magnitude of NP-signal reduction was dependent of the  
311 siRNA used (Fig 3C). Transfection of siPEPD\_1 inhibited the virus to a greater  
312 extent than siPEPD\_2 and these data are consistent with the viral titers (Fig 2)  
313 and M1 expression levels (Fig 3A) measured before. In the presence of  
314 cycloheximide, when *de novo* synthesis of NP is blocked due to inhibition of  
315 protein biosynthesis, nuclear NP signal intensity was still lower in siPEPD\_1 cells  
316 compared to control cells (Fig 3D). These data suggest that nuclear import of  
317 vRNPs is already impaired in the absence of PEPD.

### 318 **Knockdown of PEPD reduces fusion events during IAV infection.**



319 We next aimed to investigate whether the reduction of nuclear NP in PEPD  
320 knockdown cells was due to a defect in virus entry or due to a block during later  
321 events such as uncoating or transport of vRNPs into the nucleus. Therefore, we  
322 generated a dually fluorescent virus, labeled with SP-DiOC18 and R18 that  
323 allows the detection of fusion events. Both dyes are lipophilic and are inserted  
324 into the viral envelope upon labeling. This virus appears red fluorescent as the  
325 R18 dye (red) quenches the SP-DiOC18 dye (green) within the envelope of the  
326 virion (32). At the end of the viral entry process however, when viral and  
327 endosomal membranes merge, both dyes disperse within the endosomal  
328 membranes and the green fluorescent signal increases due to dequenching. To  
329 measure whether fusion is taking place in the absence of PEPD, we infected  
330 A549 cells 48h after siRNA transfection on ice with R18/SP-DiOC18-labelled  
331 A/PR/8/34. Then, cells were shifted to 37°C for 0, 90 or 180 minutes to allow  
332 entry and fusion of the labeled viruses. During the experiment, either DMSO  
333 0.1% or 10 nM bafilomycin A1 was present in the medium. Bafilomycin A1 is an  
334 inhibitor of vATPases and prevents acidification of endosomes and thus blocks  
335 IAV fusion (41). In control cells, large green fluorescent fusion sites were  
336 detectable after 90 and 180 minutes but not after 0 minutes of infection (Fig 4 A  
337 and B). Cells depleted of vATPase had a reduced number of fusion sites  
338 compared to siScr-treated cells. Also in siPEPD-transfected cells, significantly  
339 less fusion sites were counted following both, 90 minutes and 180 minutes of  
340 infection (Fig 4A and B). Treatment with bafilomycin A1 potently inhibited viral  
341 fusion in all cells tested (Fig 4C). These data strongly suggest that indeed, PEPD

342 plays a role during the IAV entry process as fusion is impaired to comparable  
343 levels to vATPase depleted cells. Thus, PEPD is required by the virus for efficient  
344 fusion or earlier during entry.

345 **PEPD is not required for attachment or internalization of IAV.**

346 We continued to identify the step affected during IAV entry in the absence of  
347 PEPD. The first step of the entry process is the attachment of the virus to the  
348 host cell membrane. To assess whether PEPD is required for receptor  
349 expression we measured the amount of both,  $\alpha 2'-3'$  and  $\alpha 2'-6'$  linked sialic acid  
350 expressed on the surface of A549 cells 48 hours after siRNA transfection. As  
351 depicted in Figure 5A, there was no difference in the amount of both types of  
352 receptors on PEPD knockdown cells compared to control cells as measured by  
353 FACS. We next investigated the effect of PEPD depletion on IAV attachment and  
354 internalization. Therefore, we generated biotinylated A/WSN/33 that can be  
355 visualized through staining with fluorescently labeled streptavidin. siPEPD or  
356 siScr transfected A549 cells were incubated on ice with this biotinylated virus,  
357 allowing only attachment of virions to the cell membrane but preventing  
358 internalization. Cell-bound virus was detected using cy3-labeled streptavidin.  
359 This signal was completely abrogated when cells were incubated with unlabeled  
360 streptavidin before fixation and subsequent staining (Fig 5B). There was no  
361 difference detectable in the amount of virus attached to cells treated with siRNAs  
362 targeting PEPD or control siRNAs. In order to measure internalized particles,  
363 virus-attached cells were incubated at 37°C for 30 minutes. Following incubation,  
364 cells were either treated with unlabeled streptavidin or PBS before fixation,

365 permeabilization and staining with cy3-labelled streptavidin. External application  
366 of unlabeled streptavidin could only partially reduce the virus-derived signal  
367 indicating that most of the virions were taken up into the cells (Fig 5B). The  
368 relative amount of internalized virus was calculated as the ratio of virus detected  
369 after 30 minutes following unlabeled streptavidin incubation to virus detected  
370 after 30 minutes washed only with PBS (Fig 5C). Notably, similar amounts of  
371 virus were internalized in siPEPD-treated cells in comparison to control cells. To  
372 confirm that virus uptake was not affected in the absence of PEPD we visualized  
373 SP-DiOC18-labeled A/WSN/33 after 30 minutes of infection. Z-stack images  
374 clearly revealed virus inside cells depleted of PEPD (Fig 5D). Taken together, we  
375 were able to demonstrate that siRNA-mediated knockdown of PEPD does neither  
376 influence IAV attachment to target cells nor virus internalization.

377 **Incoming virus exhibits a different localization pattern in PEPD depleted**  
378 **cells.**

379 Our data so far suggest that IAV requires PEPD during the entry process after  
380 internalization and before or during fusion. Next, we investigated trafficking of  
381 incoming virus particles in siRNA-treated cells deficient of PEPD. Cells were  
382 infected with A/WSN/33 with MOI of 25 and virus was visualized after 0, 30, 60,  
383 90, and 180 minutes through staining of NP which is very abundant in IAV virions  
384 (42). In control cells, IAV was detectable in the cytoplasm of infected cells at  
385 early time points (30 and 60 minutes post-infection) while after 90 and 180  
386 minutes of infection, NP was also detectable in the cell nuclei (Fig 6A). The  
387 strong signal 180 post infection was largely due to *de novo* synthesis and could

388 be abrogated through treatment with cycloheximide (data not shown).  
389 Nevertheless, similar to the data presented in Figure 3D, NP was present in the  
390 nuclei of cells in the presence of the drug, indicating that nuclear import of  
391 vRNPs was effective in siScr-transfected cells. Following PEPD knockdown  
392 however, the distribution of PEPD was largely different to control cells: The NP  
393 signal appeared predominantly in the cell periphery during all time points  
394 measured (Fig 6A). Even after 180 minutes, only few nuclei showed *de novo* NP  
395 synthesis, this is in correspondence to the data presented in Figure 3B. Instead,  
396 most of the signal was visible in proximity to the plasma-membrane of the cells.  
397 This distinctive localization pattern of NP in siPEPD-transfected cells suggests  
398 that early virus sorting and trafficking within the endosomal compartment may be  
399 affected. The morphology and localization of early and late endosomes,  
400 visualized through staining of the respective markers EEA1 and LBPA, was  
401 indistinguishable in cells treated with siPEPD or siScr (Fig 6B). In addition,  
402 staining of the endocytic machinery using lysotracker, a fluorescent dye that  
403 labels acidic organelles, did not reveal differences between siPEPD and control  
404 treated cells indicating that the endosomal compartment remains intact in the  
405 absence of PEPD (Fig 6B). We next investigated the degree of co-localization of  
406 incoming virions with early and late endosome markers in a time-course  
407 experiment (Fig 6 C-E). In control cells, NP co-localized with the early endosome  
408 marker EEA1 during early phases of infection (Fig 6D) and subsequently with the  
409 late endosomal marker LBPA (Fig 6E). In cells transfected with siRNAs targeting  
410 vATPase, a higher degree of co-localization was observed for NP and EEA1 at

411 early time points and with LBPA during late time points of infection (Fig 6D and  
412 E). This is in line with a previous report showing that depletion of vATPase  
413 results in accumulation of incoming viruses within endosomal compartments (43).  
414 In contrast, at all time points measured, less NP co-localized with either EEA1 or  
415 LBPA in PEPD deficient cells (Fig 6D and E). The retention of larger amounts of  
416 virus in the cell periphery probably largely accounts for this observation. Taken  
417 together, we demonstrate that in the absence of PEPD, incoming IAV  
418 predominantly resides in the cell periphery leading to reduced association with  
419 early and late endosomes as well as limited nuclear import and *de novo* NP  
420 synthesis.

421 **Cbz-Pro, an inhibitor of the enzymatic activity of PEPD inhibits IAV at an**  
422 **early step of the infection cycle.**

423 As PEPD possesses dipeptidase activity, we tested whether this catalytic activity  
424 mediates the proviral effects of PEPD. To this aim, we used Cbz-Pro, a  
425 competitive inhibitor of PEPD catalytic activity (44). In human fibroblasts it has  
426 been shown that 10mM of Cbz-Pro inhibits PEPD enzymatic activity to about  
427 80% (45). Therefore, we decided to use 5 and 10 mM Cbz-Pro for our  
428 experiments. Following 2h of pre-incubation, A549 cells were infected on ice with  
429 A/WSN/33, MOI=10 in the presence of the inhibitor or control treatment. Then,  
430 cells were shifted to 37°C for 3h with inhibitor present in the media. Nuclear NP  
431 expression was monitored by confocal microscopy. Cbz-Pro reduced the amount  
432 of nuclear NP compared to cells treated with the solvent methanol (Fig 7A ).  
433 Treatment with 5mM Cbz-Pro had a small but significant effect on nuclear NP-

434 synthesis, while the higher concentration strongly inhibited nuclear NP signal (Fig  
435 7A), indicating a dose-dependency. The reduction in NP signal was not due to  
436 cytotoxic effects of the inhibitor as shown in a cell viability assay for 5h treatment  
437 with the inhibitor (Fig 7B). Moreover, in the presence of cycloheximide, Cbz-Pro  
438 also reduced nuclear NP signal intensity, indicating that the inhibitor acts before  
439 viral protein synthesis (Fig 7C). We next tested whether bafilomycin A1 treatment  
440 following incubation with Cbz-Pro could maintain the inhibition of virus infection.  
441 A549 cells were incubated with Cbz-Pro for 2h prior to infection with WSN. After  
442 infection, cells were incubated in Cbz-Pro-containing medium for 1h at 37°C.  
443 Then, cells were incubated either with Cbz-Pro, solvent or bafilomycin A1. 3h  
444 post infection, nuclear NP signal intensity was measured by confocal microscopy.  
445 As shown in figure 7D, switching from Cbz-Pro treatment to bafilomycin A1 1h  
446 after infection resulted in a similar degree of inhibition as treatment with Cbz-Pro  
447 for 3h. Switching from Cbz-Pro to solvent-containing medium in turn resulted in  
448 markedly increased signal intensity of nuclear NP. These data indicate that Cbz-  
449 Pro treatment indeed targets viral entry before fusion. Taken together, our data  
450 indicate that the catalytic activity of PEPD is required for efficient entry of the  
451 virus into target cells.

452 PEPD has been shown to act as a ligand for members of the EGF receptor family  
453 when present in the extracellular space (37, 38). Furthermore, activation of  
454 EGFR has been implicated in IAV internalization (39). Therefore, we tested  
455 whether extracellularly provided recombinant PEPD can rescue virus infection  
456 following siRNA-mediated knockdown of intracellular PEPD. 48h after

457 transfection of siScr or siPEPD\_1, A549 cells were infected with IAV MOI=10 on  
458 ice and nuclear NP signal intensity was determined following incubation for 3h at  
459 37°C. It has been shown that 2.7nM PEPD suffices to activate EGFR (37). We  
460 decided to use 50nM PEPD during our experiments. Recombinant PEPD or  
461 vehicle was added to the medium either 1h before infection, during infection or  
462 1h post-infection and was maintained until the end of the experiment. As shown  
463 in figure 7E, extracellular PEPD was not able to restore nuclear NP levels in  
464 siPEPD\_1 treated cells. Thus, the effect of depletion of intracellular PEPD on IAV  
465 infection is independent of possible extracellular effects of PEPD on virus entry.

466

## 467 **Discussion**

468 In this study, we identify PEPD as a novel entry factor of IAV. We have  
469 demonstrated that upon knockdown of PEPD, IAV fusion events and the degree  
470 of co-localization with endosomal markers are strongly reduced. Instead,  
471 incoming IAV is retained in proximity to the plasma membrane. This suggests  
472 that PEPD is required for early endosomal routing of IAV during entry.

473 PEPD is a metalloprotease (46, 47) that catalyzes a rate-limiting step in the  
474 collagen-recycling pathway (48). During the degradation of collagen, PEPD  
475 cleaves dipeptides containing a proline or hydroxyproline at the C-terminus,  
476 thereby releasing free proline into the cytoplasm (48, 49). Mutations that result in  
477 loss of enzymatic activity give rise to prolylase deficiency (PD), a rare autosomal  
478 recessive disease in humans. PD is a connective tissue disorder and comprises  
479 a variety of symptoms such as mental retardation, skin ulcerations and recurrent

480 respiratory infections (48, 50-52). PEPD overexpression induces the expression  
481 of HIF-1 $\alpha$ -related gene products (53) as well as reduced NF- $\kappa$ B expression (48)  
482 thereby providing a link between PEPD and the regulation of immune responses  
483 such as cytokine production. In line with this, PD appears to be associated with  
484 systemic lupus erythematosus, an auto-immune disorder. Thus, the complexity of  
485 the disorder and the apparent distortion of barrier as well as immune functions  
486 during long-term alteration of PEPD expression and -function may explain the  
487 increased susceptibility to infections. However, PEPD has also been  
488 demonstrated to be involved in a number of signaling pathways that are activated  
489 during early phases of IAV infection: PEPD activity has been shown to be  
490 positively regulated through Integrin- $\beta$ 1 receptor signaling (54). Echistatin, a  
491 dysintegrin and receptor antagonist of Integrin- $\beta$ 1 (55), reduced PEPD activity  
492 and expression, as well as levels of phosphorylated MAPK1 and MAPK2 (56).  
493 Conversely, thrombin, an integrin activator, induced the opposite effects (56).  
494 Interestingly, MAPK1 was also shown to be activated during IAV infection in a  
495 biphasic manner (57). The early phase phosphorylation was already apparent 5-  
496 30 minutes post-infection indicating that MAPK1 signaling is involved during IAV  
497 entry. In addition, inhibition of PEPD activity with Cbz-Pro was reported to  
498 decrease phospho-AKT and phospho-mTOR levels, while incubation of cells with  
499 the PEPD products proline and hydroxyproline reversed this effect (45). The  
500 AKT/mTOR signaling cascade has also been shown to be activated early during  
501 IAV infection (58), indicating that IAV activates pathways that are positively  
502 regulated by PEPD.



503 Moreover, a recent study by Yang and colleagues suggests that PEPD can bind  
504 and activate EGFR and induce downstream signaling events (37). EGFR is a  
505 receptor tyrosine kinase (RTK) that is upstream of MAPK1 and has been  
506 implicated in IAV infection. During a recently published RNAi screen for host  
507 factors of IAV, EGFR was one of the best performing candidates (29). In addition,  
508 Eierhoff and colleagues have demonstrated that EGFR is activated following IAV  
509 attachment, which in turn promotes uptake of virions into cells (39), thereby  
510 providing evidence for a role of EGFR during IAV entry. Notably, PEPD only  
511 activated EGFR when present in the extracellular space, e.g. through release  
512 from injured cells. Similar data were obtained for ErbB2, a member of the EGF  
513 receptor family (38). Our data in contrast indicate that the enzymatic activity of  
514 PEPD may play a role for its pro-viral effects during IAV entry and that a step  
515 following internalization but before fusion is affected after PEPD depletion and  
516 inhibition of its enzymatic activity. Furthermore, our experiments using  
517 recombinant PEPD indicate that extracellularly provided PEPD cannot  
518 compensate for the depletion of intracellular PEPD and fails to rescue IAV  
519 replication in cells treated with siRNAs targeting PEPD. Thus, to what extent  
520 EGFR and other family members are involved in the PEPD-dependent regulation  
521 of IAV entry remains to be determined. Our data together with other published  
522 studies provide a link between PEPD activity, early signaling events induced by  
523 IAV and the successful completion of IAV entry. However, further experiments  
524 are required to elucidate the relationship between these events and their  
525 contribution during IAV entry.

526 Taken together, we were able to show that PEPD is required by IAV early in  
527 infection and that in the absence of PEPD early viral trafficking events are altered  
528 leading to reduced amounts of virus within early and late endosomes and fewer  
529 fusion events. While systemically, PEPD may be involved in maintaining the  
530 barrier function and immunity to infections; our data indicate that on the cellular  
531 level, PEPD is involved in orchestrating IAV routing during the entry process.  
532 Nevertheless, the precise role of PEPD during IAV entry remains elusive and the  
533 mechanism of the pro-viral role of PEPD during IAV entry will be the subject of  
534 further studies.

535

### 536 **Acknowledgements**

537 This work was supported by a grant from the Swiss National Science Foundation  
538 (31003A\_135278) to SSt. MOP is the beneficiary of a doctoral grant from the  
539 AXA Research Fund. We thank A. Helenius and Y. Yamauchi (ETH Zurich,  
540 Switzerland) for providing the protocol for the fusion assay. We also thank S.  
541 Kunz (University Hospital Lausanne, Switzerland) for providing the LASV-G  
542 expression construct.

543

544

545 **Figure legends**

546 **Figure 1. Identification of PEPD through a screen for host factors involved**  
547 **in IAV entry.**

548 **A** Overview of the screening process. **B** Positive hits of the entry screen. The  
549 darker the colour and the higher the entry score, the better was the performance  
550 of a given factor during the entry screen. **C** vATPase and PEPD depletion  
551 reduces entry of IAV VLPs. A549 cells transfected with siRNAs targeting  
552 vATPase or PEPD were infected with VLPs carrying IAV, LASV or MLV  
553 glycoproteins on their surface and encoding a luciferase reporter gene.  
554 Luciferase activity was measured at 30h post infection and luciferase of cells  
555 transfected with siScr was set to 100%. Error bars indicate standard deviation of  
556 triplicates. **D** PEPD Knockdown control. A549 cells were either transfected with  
557 siRNAs targeting PEPD or siScr alone, or co-transfected with siRNAs and a  
558 PEPD expression plasmid. PEPD protein levels after 48h were determined by  
559 western blot. Arrow indicates endogenous PEPD. Shown is a representative  
560 image of three independent experiments. **E** Cytotoxicity of PEPD-specific  
561 siRNAs 48h post-transfection. Values are relative to cells transfected with siScr.  
562 Error bars indicate standard deviation of triplicates. **F** Knockdown of PEPD does  
563 not induce MxA expression. A549 cells were transfected with siPEPD\_1 or siScr.  
564 As positive control, siScr-transfected control cells were stimulated with IFN- $\alpha$   
565 (100 U/ml) for 16h. 48h post-transfection MxA expression was measured by  
566 western blot.

567 **Figure 2. PEPD is required for growth of different IAV strains.**

568 **A** A/WSN/33 growth in A549 cells is reduced upon PEPD depletion. A549 cells  
569 were transfected with siRNAs against PEPD, NP or siScr. 48h post-transfection  
570 cells were infected with A/WSN/33 MOI=0.01. 24h post-infection, supernatants  
571 were harvested and viral growth was determined by plaque assay. Shown is one  
572 of three independent experiments performed in triplicates. Error bars indicate  
573 standard deviation. **B** Growth of A/WSN/33 in siRNA-transfected WI38 cells.  
574 Protocol as in (A) but WI38 cells were used. Virus titers were measured in tissue  
575 culture supernatants 24h and 48h post-infection. Shown is one out of three  
576 independent experiments. Error bars indicate standard deviation of triplicates. **C-**  
577 **F** Growth of different IAV strains in A549 cells transfected with siScr, siPEPD\_1  
578 or siVATPase. 48h post-transfection, cells were infected with FPV/Dobson  
579 (H7N7) with MOI=0.01 (C), A/Hong Kong/68 (H3N2) with MOI=1 (D),  
580 A/Netherlands/602/2009 (H1N1) with MOI=1 (E) or A/Panama/2007/99 (H3N2)  
581 with MOI=1 (F). 24h later, supernatants were harvested and viral titers were  
582 determined by plaque assay. Shown is one out of three independent experiments  
583 performed in duplicates. Error bars indicate standard deviation.

584 **Figure 3. Depletion of PEPD affects an early step of the IAV life cycle.**

585 **A** Early M1 expression is reduced by PEPD knockdown. A549 cells were  
586 transfected with siRNAs targeting PEPD or siScr. 48h post-transfection, cells  
587 were infected with A/WSN/33 MOI=1. 6h after infection, cells were lysed and M1  
588 expression was determined by western blot. **B** Immunofluorescence pictures

589 showing reduced nuclear NP signal in PEPD knockdown cells. siRNA transfected  
590 A549 were infected on ice with A/WSN/33 MOI=10 for 1h. Then, cells were  
591 incubated at 37°C for additional 3h. Cells were stained for NP expression (green)  
592 and nuclei (blue) and analyzed by confocal microscopy. Scale bars equal 25  $\mu$ m.  
593 Shown are representative pictures of three independent experiments performed  
594 in duplicates. **C** Quantification of (B). Nuclear NP signal intensity of 100 nuclei  
595 per condition was quantified using ImageJ software and analyzed using the  
596 Mann-Whitney test. Error bars indicate standard deviation. **D** Quantification of  
597 imported nuclear NP. Experimental set-up as in (B) but during the experiment,  
598 cycloheximide (100ug/ml) was present in the media. 87 nuclei were counted per  
599 condition and analyzed using the Mann-Whitney test. Error bars indicate  
600 standard deviation.

601 **Figure 4. Knockdown of PEPD reduces fusion events during IAV infection.**

602 **A** Reduced fusion of SP-DiOC18/R18-labelled virus in PEPD-depleted cells.  
603 A549 cells were transfected with siRNAs targeting PEPD, vATPase or with siScr.  
604 48h post-transfection cells were first pre-incubated with 10 nM bafilomycin A1 or  
605 0.1% DMSO and then infected on ice with SP-DiOC18/R18-labelled A/PR/8/34  
606 for 1h. After incubation at 37°C for 0, 90 or 180 min cells were analyzed by  
607 confocal microscopy. Shown are images representative of the 90 minutes time  
608 point from the DMSO-treated samples. Scale bars equal 10  $\mu$ m. **B and C**  
609 Quantification of (A).The number of fusion sites per cell was quantified using  
610 ImageJ software. Cells treated with DMSO are shown in (B). Cells treated with

611 bafilomycin A1 (10nM) are depicted in (C). (B) and (C) show a quantification of  
612 one out of three independent experiments. Error bars indicate standard deviation.

613 **Figure 5. Effect of PEPD knockdown on sialic acid expression, IAV**  
614 **attachment and uptake.**

615 **A** PEPD knockdown does not influence surface sialic acid expression. A549 cells  
616 were treated with siRNAs against PEPD or with siScr, stained with *Sambucus*  
617 *nigra* or *Maackia amurensis* lectins recognizing either  $\alpha 2'-3'$  or  $\alpha 2'-6'$  sialic acid  
618 and analyzed by FACS. Shown is one out of three independent experiments. Per  
619 condition, 10000 cells were analyzed. **B and C** Virus attachment and  
620 internalization are not affected by PEPD knockdown. A549 cells were transfected  
621 with siRNAs targeting PEPD or siScr and were infected 48h later on ice with  
622 biotinylated A/WSN/33 for 1h. Cells were either fixed following infection or, virus  
623 was allowed to internalize for 30 minutes at 37°C. In half of the samples plasma  
624 membrane-attached virus was masked using unlabeled streptavidin before  
625 permeabilization (+ strep). The other half was PBS treated. Following  
626 permeabilization, cells were stained with Cy3-labelled streptavidin and analyzed  
627 by FACS (B). The relative amount of internalized virus was calculated as the ratio  
628 of virus-positive cells at ,30 min + strep' to ,30 min without strep' (C). Shown is  
629 one out of three independent experiments. Per condition, 10000 cells were  
630 analyzed. **D** Visualization of IAV internalization. SP-DiOC18-labelled IAV was  
631 allowed to cold-bind to siScr or siPEPD treated A549 cells. Then, temperature  
632 was shifted to 37°C. After 30 minutes, cells were fixed and  $\alpha 2'-6'$  linked sialic  
633 acid on the cell surface was stained using *Sambucus nigra* lectin. Images were

634 taken using confocal microscopy. Scale bars equal 10  $\mu$ m. Arrows indicate  
635 DiOC18-labeled, internalized virus. Representative images are shown.

636 **Figure 6. Incoming virus exhibits a different localization-pattern in PEPD**  
637 **knockdown cells.**

638 **A** Immunofluorescence pictures showing NP distribution in PEPD-depleted and  
639 control cells. A549 cells were transfected with siScr or siPEPD\_1. 48 hours post-  
640 transfection, cells were infected with A/WSN/33 with MOI=25. At the indicated  
641 time points, cells were fixed, stained for viral NP and analyzed by confocal  
642 microscopy. Scale bars equal 25  $\mu$ m. Shown is one out of three independent  
643 experiments. **B** Effect of PEPD knockdown on the morphology of the endocytic  
644 machinery. siRNA-transfected A549 cells were either stained for EEA1 or LBPA  
645 or incubated with lysotracker reagent. Scale bars equal 10  $\mu$ m. Representative  
646 images of two independent experiments are shown. **C** Incoming viruses display  
647 less co-localization with endosomes in PEPD-depleted cells. Experimental set-up  
648 as in (A). Cells were co-stained against NP (green) and either EEA1 or LBPA  
649 (red). Shown are representative images of virus-infected cells after 30 minutes  
650 (EEA1) or 60 minutes (LBPA). Scale bars equal 10  $\mu$ m. **D and E** Co-localization  
651 quantification of the EEA1 (D) and LBPA (E) staining. Confocal images were  
652 analyzed for co-localization using Imaris software. The Mann-Whitney test was  
653 used to test for statistical significance (siScr vs. siPEPD\_1). Shown is one out of  
654 three independent experiments. Error bars indicate standard deviation.

655 **Figure 7. Inhibition of PEPD enzymatic function restricts IAV early in**  
656 **infection.**

657 **A** Nuclear NP expression in Cbz-Pro-treated cells. A549 cells were pre-treated  
658 for 2h with indicated amounts of Cbz-Pro or the solvent 0.5% MetOH. Cells were  
659 infected on ice with A/WSN/33 MOI=10 and afterwards shifted to 37°C for  
660 additional 3h. During infection and later incubation the respective compounds  
661 were present in the media. Cells were stained against NP and analyzed by  
662 confocal microscopy. Mean nuclear intensity was quantified using Image J  
663 software. Mann-Whitney test was used for statistical comparison. Shown is one  
664 of three independent experiments. Error bars indicate standard deviation of 100  
665 quantified nuclei. **B** Cell viability. Cytotoxic effects of Cbz-Pro treatment were  
666 assessed in A549 cells following incubation for 5h. **C** Effect of Cbz-Pro on  
667 nuclear NP levels in the presence of cycloheximide. Experimental set-up as in  
668 (A). MOI=50 was used for infection and 100 ug/ml cycloheximide-containing  
669 medium was added after infection. **D** Sequential treatment with Cbz-Pro and  
670 bafilomycin A1 inhibits nuclear NP expression. A549 cells were pre-incubated  
671 with 10mM Cbz-Pro or 0.5% MetOH for 2h before infection on ice with A/WSN/33  
672 MOI=10 in the presence of the inhibitor or solvent. After infection, cells were  
673 shifted to 37°C for 3h. 1h post-infection, Cbz-Pro or MetOH was present in the  
674 media. Following 30 min of incubation with both, Cbz-Pro and bafilomycin A1  
675 (10nM) or MetOH, cells were further incubated with bafilomycin A1 or MetOH-  
676 containing medium for additional 90 min. Nuclear NP was measured and  
677 quantified as described above. Shown is one out of three independent



678 experiments with error bars indicating standard deviation of 100 analyzed nuclei.  
679 **E** Extracellular PEPD cannot rescue IAV infection in siPEPD-treated cells. A549  
680 cells were transfected with siScr or siPEPD\_1. 48h post-transfection, cells were  
681 treated with 50nM of recombinant PEPD 1h before, 1h after or during infection  
682 with A/WSN/33 MOI=10. Following addition, PEPD was present in the media until  
683 3h after infection. Nuclear NP was measured and analyzed as described above.  
684 Shown is one out of three independent experiments with error bars indicating  
685 standard deviation of 100 quantified nuclei.

686

687 **References**

- 688 1. **Palese, P., and M. L. Shaw.** 2007. Orthomyxoviridae: The viruses and  
689 their replication. *In* D. M. Knipe and P. M. Howley (ed.), *Fields Virology*,  
690 5th ed, vol. 2. Lippincott Williams and Wilkins, Philadelphia.
- 691 2. **Wise, H. M., E. C. Hutchinson, B. W. Jagger, A. D. Stuart, Z. H. Kang,**  
692 **N. Robb, L. M. Schwartzman, J. C. Kash, E. Fodor, A. E. Firth, J. R.**  
693 **Gog, J. K. Taubenberger, and P. Digard.** 2012. Identification of a novel  
694 splice variant form of the influenza A virus M2 ion channel with an  
695 antigenically distinct ectodomain. *PLoS pathogens* **8**:e1002998.
- 696 3. **Baum, L. G., and J. C. Paulson.** 1990. Sialyloligosaccharides of the  
697 respiratory epithelium in the selection of human influenza virus receptor  
698 specificity. *Acta Histochem Suppl* **40**:35-38.
- 699 4. **Edinger, T. O., M. O. Pohl, and S. Stertz.** 2014. Entry of influenza A  
700 virus: host factors and antiviral targets. *J Gen Virol* **95**:263-277.
- 701 5. **Patterson, S., J. S. Oxford, and R. R. Dourmashkin.** 1979. Studies on  
702 the mechanism of influenza virus entry into cells. *J Gen Virol* **43**:223-229.
- 703 6. **Matlin, K. S., H. Reggio, A. Helenius, and K. Simons.** 1981. Infectious  
704 entry pathway of influenza virus in a canine kidney cell line. *The Journal of*  
705 *cell biology* **91**:601-613.
- 706 7. **Yoshimura, A., K. Kuroda, K. Kawasaki, S. Yamashina, T. Maeda, and**  
707 **S. Ohnishi.** 1982. Infectious cell entry mechanism of influenza virus.  
708 *Journal of virology* **43**:284-293.
- 709 8. **de Vries, E., D. M. Tscherne, M. J. Wienholts, V. Cobos-Jimenez, F.**  
710 **Scholte, A. Garcia-Sastre, P. J. Rottier, and C. A. de Haan.** 2011.  
711 Dissection of the influenza A virus endocytic routes reveals  
712 macropinocytosis as an alternative entry pathway. *PLoS pathogens*  
713 **7**:e1001329.
- 714 9. **Sieczkarski, S. B., and G. R. Whittaker.** 2002. Influenza virus can enter  
715 and infect cells in the absence of clathrin-mediated endocytosis. *Journal of*  
716 *virology* **76**:10455-10464.
- 717 10. **Maeda, T., and S. Ohnishi.** 1980. Activation of influenza virus by acidic  
718 media causes hemolysis and fusion of erythrocytes. *FEBS Lett* **122**:283-  
719 287.
- 720 11. **Daniels, R. S., J. C. Downie, A. J. Hay, M. Knossow, J. J. Skehel, M. L.**  
721 **Wang, and D. C. Wiley.** 1985. Fusion mutants of the influenza virus  
722 hemagglutinin glycoprotein. *Cell* **40**:431-439.
- 723 12. **White, J. M., and I. A. Wilson.** 1987. Anti-peptide antibodies detect steps  
724 in a protein conformational change: low-pH activation of the influenza virus  
725 hemagglutinin. *The Journal of cell biology* **105**:2887-2896.
- 726 13. **Wharton, S. A., R. B. Belshe, J. J. Skehel, and A. J. Hay.** 1994. Role of  
727 virion M2 protein in influenza virus uncoating: specific reduction in the rate  
728 of membrane fusion between virus and liposomes by amantadine. *J Gen*  
729 *Virol* **75 ( Pt 4)**:945-948.

- 730 14. **Zhirnov, O. P.** 1990. Solubilization of matrix protein M1/M from virions  
731 occurs at different pH for orthomyxo- and paramyxoviruses. *Virology*  
732 **176**:274-279.
- 733 15. **O'Neill, R., R. Jaskunas, G. Blobel, P. Palese, and J. Moroianu.** 1995.  
734 Nuclear import of influenza virus RNA can be mediated by viral  
735 nucleoprotein and transport factors required for protein import.  
736 *J.Biol.Chem.* **270**:22701-22704.
- 737 16. **Davies, W. L., R. R. Grunert, R. F. Haff, J. W. McGahen, E. M.**  
738 **Neumayer, M. Paulshock, J. C. Watts, T. R. Wood, E. C. Hermann, and**  
739 **C. E. Hoffmann.** 1964. Antiviral Activity of 1-Adamantanamine  
740 (Amantadine). *Science* **144**:862-863.
- 741 17. **Skehel, J. J., A. J. Hay, and J. A. Armstrong.** 1978. On the mechanism  
742 of inhibition of influenza virus replication by amantadine hydrochloride. *J*  
743 *Gen Virol* **38**:97-110.
- 744 18. **Hay, A. J., A. J. Wolstenholme, J. J. Skehel, and M. H. Smith.** 1985.  
745 The molecular basis of the specific anti-influenza action of amantadine.  
746 *Embo J* **4**:3021-3024.
- 747 19. **Kim, C. U., W. Lew, M. A. Williams, H. Liu, L. Zhang, S. Swaminathan,**  
748 **N. Bischofberger, M. S. Chen, D. B. Mendel, C. Y. Tai, W. G. Laver,**  
749 **and R. C. Stevens.** 1997. Influenza neuraminidase inhibitors possessing  
750 a novel hydrophobic interaction in the enzyme active site: design,  
751 synthesis, and structural analysis of carbocyclic sialic acid analogues with  
752 potent anti-influenza activity. *Journal of the American Chemical Society*  
753 **119**:681-690.
- 754 20. **Vonitzstein, M., W. Y. Wu, G. B. Kok, M. S. Pegg, J. C. Dyason, B. Jin,**  
755 **T. V. Phan, M. L. Smythe, H. F. White, S. W. Oliver, P. M. Colman, J. N.**  
756 **Varghese, D. M. Ryan, J. M. Woods, R. C. Bethell, V. J. Hotham, J. M.**  
757 **Cameron, and C. R. Penn.** 1993. Rational Design of Potent Sialidase-  
758 Based Inhibitors of Influenza Virus Replication. *Nature* **363**:418-423.
- 759 21. **Bright, R. A., M. J. Medina, X. Xu, G. Perez-Oroz, T. R. Wallis, X. M.**  
760 **Davis, L. Povinelli, N. J. Cox, and A. I. Klimov.** 2005. Incidence of  
761 adamantane resistance among influenza A (H3N2) viruses isolated  
762 worldwide from 1994 to 2005: a cause for concern. *Lancet* **366**:1175-  
763 1181.
- 764 22. **Ison, M. G.** 2011. Antivirals and resistance: influenza virus. *Current*  
765 *opinion in virology* **1**:563-573.
- 766 23. **Hao, L., A. Sakurai, T. Watanabe, E. Sorensen, C. A. Nidom, M. A.**  
767 **Newton, P. Ahlquist, and Y. Kawaoka.** 2008. Drosophila RNAi screen  
768 identifies host genes important for influenza virus replication. *Nature*  
769 **454**:890-893.
- 770 24. **Brass, A. L., I. C. Huang, Y. Benita, S. P. John, M. N. Krishnan, E. M.**  
771 **Feeley, B. J. Ryan, J. L. Weyer, L. van der Weyden, E. Fikrig, D. J.**  
772 **Adams, R. J. Xavier, M. Farzan, and S. J. Elledge.** 2009. The IFITM  
773 proteins mediate cellular resistance to influenza A H1N1 virus, West Nile  
774 virus, and dengue virus. *Cell* **139**:1243-1254.

- 775 25. **Shapira, S. D., I. Gat-Viks, B. O. Shum, A. Dricot, M. M. de Grace, L.**  
776 **Wu, P. B. Gupta, T. Hao, S. J. Silver, D. E. Root, D. E. Hill, A. Regev,**  
777 **and N. Hacohen.** 2009. A physical and regulatory map of host-influenza  
778 interactions reveals pathways in H1N1 infection. *Cell* **139**:1255-1267.
- 779 26. **Karlas, A., N. Machuy, Y. Shin, K. P. Pleissner, A. Artarini, D. Heuer,**  
780 **D. Becker, H. Khalil, L. A. Ogilvie, S. Hess, A. P. Maurer, E. Muller, T.**  
781 **Wolff, T. Rudel, and T. F. Meyer.** 2010. Genome-wide RNAi screen  
782 identifies human host factors crucial for influenza virus replication. *Nature*  
783 **463**:818-822.
- 784 27. **Watanabe, T., S. Watanabe, and Y. Kawaoka.** 2010. Cellular networks  
785 involved in the influenza virus life cycle. *Cell host & microbe* **7**:427-439.
- 786 28. **Konig, R., S. Stertz, Y. Zhou, A. Inoue, H. H. Hoffmann, S.**  
787 **Bhattacharyya, J. G. Alamares, D. M. Tscherne, M. B. Ortigoza, Y.**  
788 **Liang, Q. Gao, S. E. Andrews, S. Bandyopadhyay, P. De Jesus, B. P.**  
789 **Tu, L. Pache, C. Shih, A. Orth, G. Bonamy, L. Miraglia, T. Ideker, A.**  
790 **Garcia-Sastre, J. A. Young, P. Palese, M. L. Shaw, and S. K. Chanda.**  
791 2010. Human host factors required for influenza virus replication. *Nature*  
792 **463**:813-817.
- 793 29. **Su, W. C., Y. C. Chen, C. H. Tseng, P. W. Hsu, K. F. Tung, K. S. Jeng,**  
794 **and M. M. Lai.** 2013. Pooled RNAi screen identifies ubiquitin ligase Itch as  
795 crucial for influenza A virus release from the endosome during virus entry.  
796 *Proc Natl Acad Sci U S A* **110**:17516-17521.
- 797 30. **Ward, S. E., H. S. Kim, K. Komurov, S. Mendiratta, P. L. Tsai, M.**  
798 **Schmolke, N. Satterly, B. Manicassamy, C. V. Forst, M. G. Roth, A.**  
799 **Garcia-Sastre, K. M. Blazewska, C. E. McKenna, B. M. Fontoura, and**  
800 **M. A. White.** 2012. Host modulators of H1N1 cytopathogenicity. *PLoS*  
801 *One* **7**:e39284.
- 802 31. **Stertz, S., and M. L. Shaw.** 2011. Uncovering the global host cell  
803 requirements for influenza virus replication via RNAi screening. *Microbes*  
804 *Infect* **13**:516-525.
- 805 32. **Sakai, T., M. Ohuchi, M. Imai, T. Mizuno, K. Kawasaki, K. Kuroda, and**  
806 **S. Yamashina.** 2006. Dual wavelength imaging allows analysis of  
807 membrane fusion of influenza virus inside cells. *Journal of virology*  
808 **80**:2013-2018.
- 809 33. **Pasqual, G., J. M. Rojek, M. Masin, J. Y. Chatton, and S. Kunz.** 2011.  
810 Old world arenaviruses enter the host cell via the multivesicular body and  
811 depend on the endosomal sorting complex required for transport. *PLoS*  
812 *pathogens* **7**:e1002232.
- 813 34. **McClure, M. O., M. A. Sommerfelt, M. Marsh, and R. A. Weiss.** 1990.  
814 The pH independence of mammalian retrovirus infection. *J Gen Virol* **71** (  
815 **Pt 4**):767-773.
- 816 35. **Perez, L., and L. Carrasco.** 1994. Involvement of the vacuolar H(+)-  
817 ATPase in animal virus entry. *J Gen Virol* **75** (**Pt 10**):2595-2606.
- 818 36. **Galloway, C. J., G. E. Dean, M. Marsh, G. Rudnick, and I. Mellman.**  
819 1983. Acidification of macrophage and fibroblast endocytic vesicles in  
820 vitro. *Proc Natl Acad Sci U S A* **80**:3334-3338.

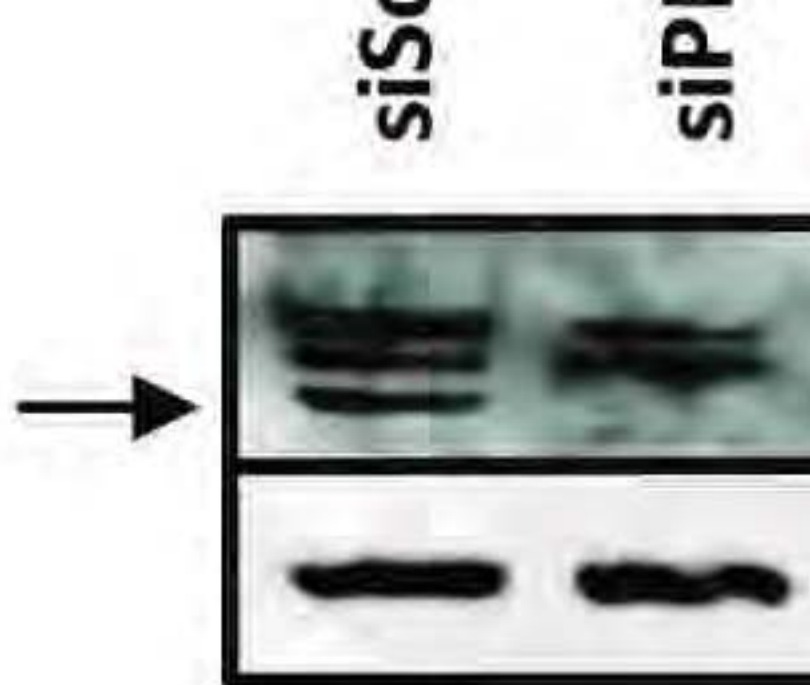
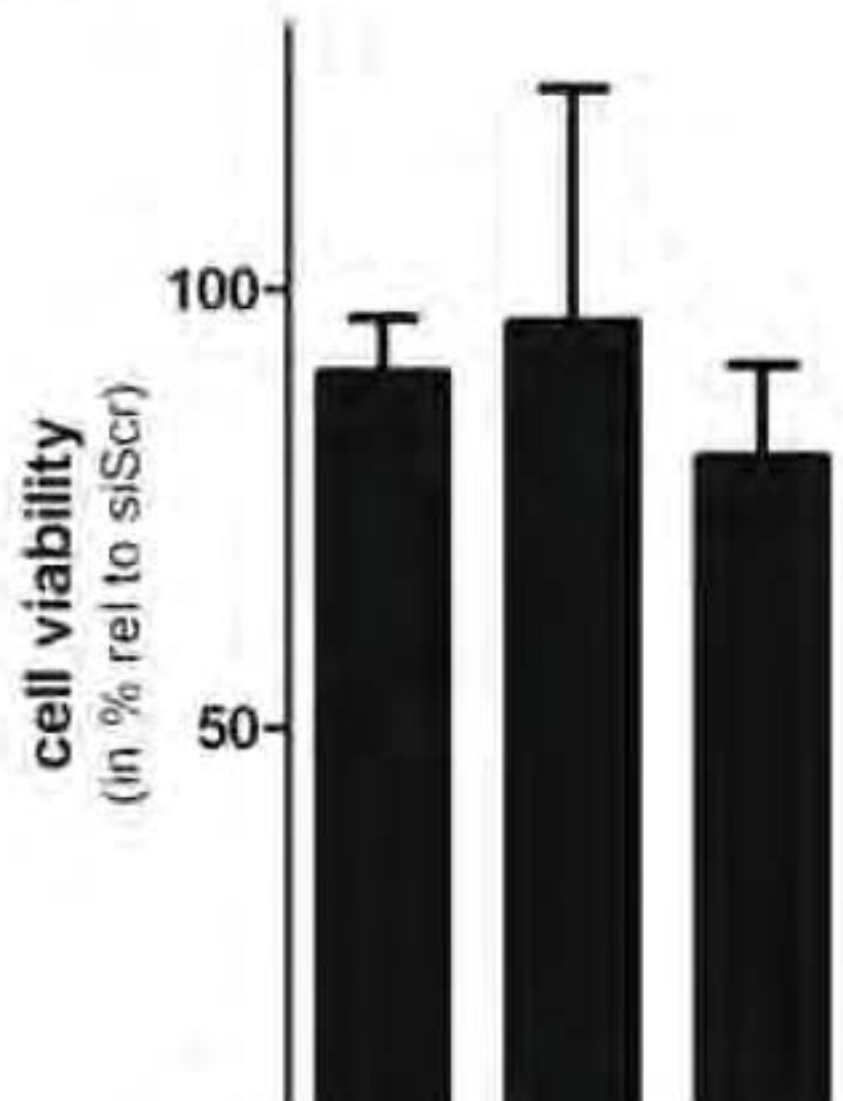
- 821 37. **Yang, L., Y. Li, Y. Ding, K. S. Choi, A. L. Kazim, and Y. Zhang.** 2013.  
822 Prolidase directly binds and activates epidermal growth factor receptor  
823 and stimulates downstream signaling. *The Journal of biological chemistry*  
824 **288**:2365-2375.
- 825 38. **Yang, L., Y. Li, and Y. Zhang.** 2014. Identification of prolidase as a high  
826 affinity ligand of the ErbB2 receptor and its regulation of ErbB2 signaling  
827 and cell growth. *Cell death & disease* **5**:e1211.
- 828 39. **Eierhoff, T., E. R. Hrinčius, U. Rescher, S. Ludwig, and C. Ehrhardt.**  
829 2010. The epidermal growth factor receptor (EGFR) promotes uptake of  
830 influenza A viruses (IAV) into host cells. *PLoS pathogens* **6**:e1001099.
- 831 40. **Zona, L., J. Lupberger, N. Sidahmed-Adrar, C. Thumann, H. J. Harris,**  
832 **A. Barnes, J. Florentin, R. G. Tawar, F. Xiao, M. Turek, S. C. Durand,**  
833 **F. H. Duong, M. H. Heim, F. L. Cosset, I. Hirsch, D. Samuel, L. Brino,**  
834 **M. B. Zeisel, F. Le Naour, J. A. McKeating, and T. F. Baumert.** 2013.  
835 HRas signal transduction promotes hepatitis C virus cell entry by  
836 triggering assembly of the host tetraspanin receptor complex. *Cell host &*  
837 *microbe* **13**:302-313.
- 838 41. **Guinea, R., and L. Carrasco.** 1995. Requirement for vacuolar proton-  
839 ATPase activity during entry of influenza virus into cells. *Journal of*  
840 *virology* **69**:2306-2312.
- 841 42. **Inglis, S. C., A. R. Carroll, R. A. Lamb, and B. W. Mahy.** 1976.  
842 Polypeptides specified by the influenza virus genome I. Evidence for eight  
843 distinct gene products specified by fowl plague virus. *Virology* **74**:489-503.
- 844 43. **Huotari, J., N. Meyer-Schaller, M. Hubner, S. Stauffer, N. Katheder, P.**  
845 **Horvath, R. Mancini, A. Helenius, and M. Peter.** 2012. Cullin-3 regulates  
846 late endosome maturation. *Proc Natl Acad Sci U S A* **109**:823-828.
- 847 44. **Lupi, A., A. Rossi, P. Vaghi, A. Gallanti, G. Cetta, and A. Forlino.** 2005.  
848 N-benzyloxycarbonyl-L-proline: an in vitro and in vivo inhibitor of prolidase.  
849 *Biochimica et biophysica acta* **1744**:157-163.
- 850 45. **Surazynski, A., W. Miltyk, I. Prokop, and J. Palka.** 2010. Prolidase-  
851 dependent regulation of TGF beta (corrected) and TGF beta receptor  
852 expressions in human skin fibroblasts. *European journal of pharmacology*  
853 **649**:115-119.
- 854 46. **Mock, W. L., and P. C. Green.** 1990. Mechanism and inhibition of  
855 prolidase. *The Journal of biological chemistry* **265**:19606-19610.
- 856 47. **Lowther, W. T., and B. W. Matthews.** 2002. Metalloaminopeptidases:  
857 common functional themes in disparate structural surroundings. *Chemical*  
858 *reviews* **102**:4581-4608.
- 859 48. **Surazynski, A., W. Miltyk, J. Palka, and J. M. Phang.** 2008. Prolidase-  
860 dependent regulation of collagen biosynthesis. *Amino acids* **35**:731-738.
- 861 49. **Kitchener, R. L., and A. M. Grunden.** 2012. Prolidase function in proline  
862 metabolism and its medical and biotechnological applications. *Journal of*  
863 *applied microbiology* **113**:233-247.
- 864 50. **Powell, G. F., M. A. Rasco, and R. M. Maniscalco.** 1974. A prolidase  
865 deficiency in man with iminopeptiduria. *Metabolism: clinical and*  
866 *experimental* **23**:505-513.

- 867 51. **Freij, B. J., H. L. Levy, G. Dudin, D. Mutasim, M. Deeb, and V. M. Der**  
868 **Kaloustian.** 1984. Clinical and biochemical characteristics of prolidase  
869 deficiency in siblings. *American journal of medical genetics* **19**:561-571.
- 870 52. **Isemura, M., T. Hanyu, F. Gejyo, R. Nakazawa, R. Igarashi, S. Matsuo,**  
871 **K. Ikeda, and Y. Sato.** 1979. Prolidase deficiency with imidodipeptiduria.  
872 A familial case with and without clinical symptoms. *Clinica chimica acta;*  
873 *international journal of clinical chemistry* **93**:401-407.
- 874 53. **Surazynski, A., S. P. Donald, S. K. Cooper, M. A. Whiteside, K.**  
875 **Salnikow, Y. Liu, and J. M. Phang.** 2008. Extracellular matrix and HIF-1  
876 signaling: the role of prolidase. *International journal of cancer. Journal*  
877 *international du cancer* **122**:1435-1440.
- 878 54. **Palka, J. A., and J. M. Phang.** 1997. Prolidase activity in fibroblasts is  
879 regulated by interaction of extracellular matrix with cell surface integrin  
880 receptors. *Journal of cellular biochemistry* **67**:166-175.
- 881 55. **Sato, M., M. K. Sardana, W. A. Grasser, V. M. Garsky, J. M. Murray,**  
882 **and R. J. Gould.** 1990. Echistatin is a potent inhibitor of bone resorption  
883 in culture. *The Journal of cell biology* **111**:1713-1723.
- 884 56. **Surazynski, A., P. Sienkiewicz, S. Wolczynski, and J. Palka.** 2005.  
885 Differential effects of echistatin and thrombin on collagen production and  
886 prolidase activity in human dermal fibroblasts and their possible  
887 implication in beta1-integrin-mediated signaling. *Pharmacological research*  
888 *: the official journal of the Italian Pharmacological Society* **51**:217-221.
- 889 57. **Pleschka, S., T. Wolff, C. Ehrhardt, G. Hobom, O. Planz, U. R. Rapp,**  
890 **and S. Ludwig.** 2001. Influenza virus propagation is impaired by inhibition  
891 of the Raf/MEK/ERK signalling cascade. *Nat Cell Biol* **3**:301-305.
- 892 58. **Ehrhardt, C., T. Wolff, S. Pleschka, O. Planz, W. Beermann, J. G.**  
893 **Bode, M. Schmolke, and S. Ludwig.** 2007. Influenza A virus NS1 protein  
894 activates the PI3K/Akt pathway to mediate antiapoptotic signaling  
895 responses. *Journal of virology* **81**:3058-3067.

896

897

**E**





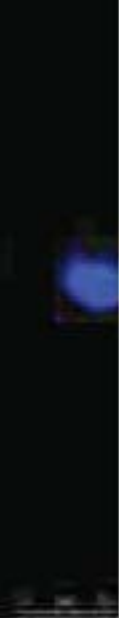
IVATPase

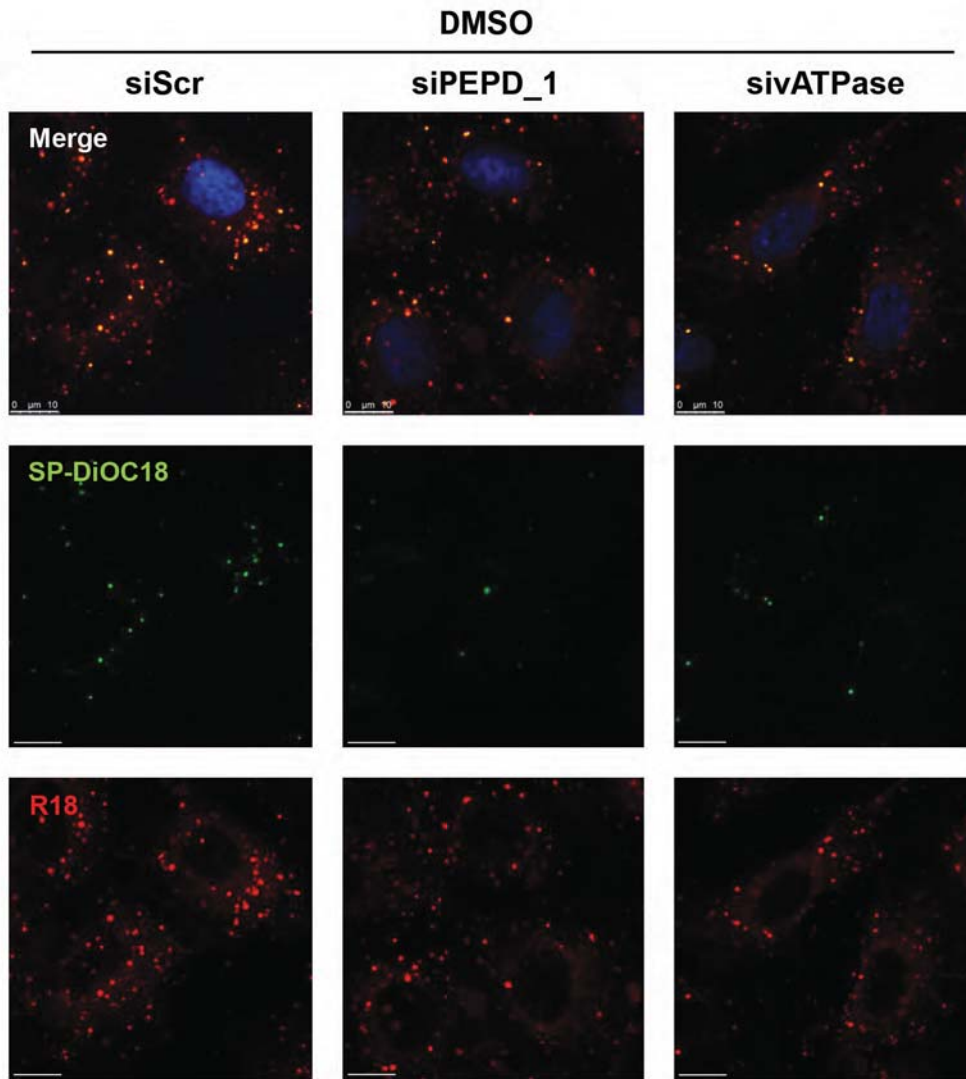
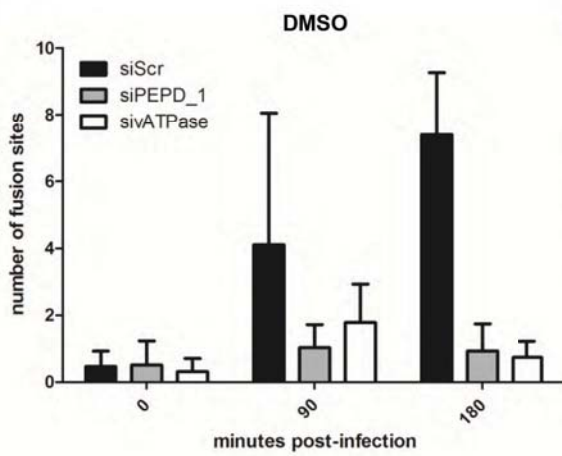
007/99



IVATPase





**A****B****C**